Geochemistry Geophysics Geosystems G3
AN ELECTRONIC JOURNAL OF THE EARTH SCIENCES
Published by AGU and the Geochemical Society

Article
Volume 4, Number 7
9 July 2003
1055, doi:10.1029/2002GC000336
ISSN: 1525-2027

Extreme chemical variability as a consequence of channelized melt transport

Marc Spiegelman
Lamont-Doherty Earth Observatory of Columbia University, Route 9W, Palisades, New York 10964, USA (mspieg@ldeo.columbia.edu)

Peter B. Kelemen
Woods Hole Oceanographic Institute, Woods Hole, Massachusetts 02543, USA (peterk@whoi.edu)

[1] The spatial and temporal variability of chemical signals in lavas, residues, and melt inclusions provides important constraints on source heterogeneity, the efficiency of convection, and melt transport processes in the mantle. The past decade has seen an impressive increase in the number, precision, and spatial resolution of chemical analyses. However, as resolution has increased, the picture of variation that emerges has become increasingly difficult to understand. For example, mid-ocean ridge basalts can display large variations in trace element concentration on scales from 1000 km of ridge to melt inclusions in 500 micron crystals. These observations suggest that melt transport processes do not readily homogenize partially molten regions. While some of the observed variability is due to source variations, a large proportion could be the consequence of magma transport in channelized systems. We present results of numerical models that calculate the trace element signatures of high-porosity dissolution channels produced by reactive fluid flow. These models were originally developed to explain the organization of melt transport networks, based on observations of "replacive dunites" found in ophiolites. Channelized flow can produce orders of magnitude variation in the concentrations of highly incompatible elements, even for idealized systems with a homogeneous source, constant bulk partition coefficients, and equilibrium transport. Most importantly, the full range of variability may be found in each channel because channelization can transpose the chemical variability produced by melting throughout the melting column into horizontal variability across the width of the channel. The centers of channels contain trace element–enriched melts from depth, while the edges of the channels transport highly depleted melts extracted from the interchannel regions at shallower levels. As dunite channels may be spaced on scales of 1–100 m in the mantle, this mechanism allows highly variable melt compositions to be delivered to the Moho on small length scales. The chemical variation produced in the models is consistent with that seen in melt inclusion suites, lavas, and residual mantle peridotites dredged from the ridges and sampled in ophiolites.

Components: 8161 words, 9 figures, 1 table, 1 dataset.

Keywords: reactive flow modeling; magma dynamics; trace elements.

Index Terms: 8434 Volcanology: Magma migration; 3210 Mathematical Geophysics: Modeling; 1065 Geochemistry: Trace elements (3670); 3035 Marine Geology and Geophysics: Midocean ridge processes.

Received 28 February 2002; **Revised** 12 December 2002; **Accepted** 16 December 2002; **Published** 9 July 2003.

Spiegelman, M., and P. B. Kelemen, Extreme chemical variability as a consequence of channelized melt transport, *Geochem. Geophys. Geosyst.*, *4*(7), 1055, doi:10.1029/2002GC000336, 2003.

1. Introduction

[2] The natural variation of chemical composition of primitive melts, melt inclusions and residual mantle peridotites is one of the primary sources of information on convection, melting, and melt transport processes in the mantle. The past decade has seen a significant increase in the number, precision and spatial resolution of chemical analyses. However, as we sample at smaller and smaller scales, the compositional variability of mantle materials does not seem to diminish. For example, the trace element variability in lavas erupted over 1000 km of ridge axis is comparable to that seen in suites of melt inclusions within individual hand-samples. The observation of large chemical variability at small scales implies that melt transport in partially molten regions is inefficient at mixing melts. One possible explanation is that melt transport occurs in a channelized network that limits interaction between melt and solid. While this assumption is implicit in many commonly used geochemical models (reviewed below), these models do not explicitly account for the mechanism of melt transport. Thus the physical mechanisms of network formation and melt transport, and their effect on chemical variation, remain poorly understood.

[3] This paper explores the chemical consequences of new physical models of channelized melt transport [*Spiegelman et al.*, 2001] (http://www.ldeo.columbia.edu/~mspieg/ReactiveFlow/). Significant compositional variability can be produced by the melt extraction process alone, even for idealized homogeneous systems. These models are consistent with observations, producing extreme chemical variability on very small length scales. These results are a natural consequence of melt transport processes and provide physical explanations for some of the least understood observations of chemical variability.

1.1. Evidence for Channelized Flow: Compositional Variability in Mid-Ocean Ridge Melts

1.1.1. Melt Inclusion Studies

[4] Chief among the puzzling new observations are the results of melt inclusion studies [e.g., *Sobolev and Shimizu*, 1993; *Nielsen et al.*, 1995; *Sobolev*, 1996; *Shimizu and Grove*, 1998; *Shimizu*, 1998; *Saal et al.*, 1998; *Sours-Page et al.*, 1999; *Sobolev et al.*, 2000; *Slater et al.*, 2001]. These studies show extreme variability in both trace elements and isotope ratios in individual hand samples and in some cases between inclusions within the same crystal. Figure 1, for example, shows a summary of rare earth patterns from melt inclusions trapped in high-Mg olivine phenocrysts from three hand-samples from the Mid-Atlantic Ridge. These inclusions show 1–2 orders of magnitude concentration variation in La and about a factor of 2 variation in Yb. These samples include distinct, "ultra-depleted" melt inclusions with compositions that are not found among the erupted host lavas [*Sobolev and Shimizu*, 1993]. Similar results for Iceland [*Slater et al.*, 2001] also show large variability of melt inclusions within individual flows from Theistareykir shield volcano. The most trace element–enriched inclusions are ~2–4 times more enriched than their host lavas. The Iceland data also show a distinct tail of very depleted inclusions.

[5] Olivine hosted melt inclusions are thought to be trapped during crystallization in the crust at moderate to low pressures [e.g., *Sobolev*, 1996]. If so, then the large variability in hand samples implies that melts found near the Moho are heterogeneous on small length scales. This requires some mechanism for delivering melts to the Moho without significant homogenization during melt transport. The reduction in variability between melt inclusions and host lavas would arise from crustal processes such as mixing in magma chambers and flow in dikes.

1.1.2. Variability in MORB Lavas

[6] Larger scale sampling also yields compositionally variable lavas over short spatial scales. For example, at 12°N on the East Pacific Rise [*Reynolds et al.*, 1992; *Reynolds*, 1995; *Reynolds and Langmuir*, 2000] lavas with compositionally distinct parental magmas can be sampled within 500 m of each other within the axial summit graben. Other studies at 9°N EPR [e.g., *Perfit et al.*, 1994a, 1994b; *Perfit and Chadwick*, 1998] show more modest variations and the overall variability of

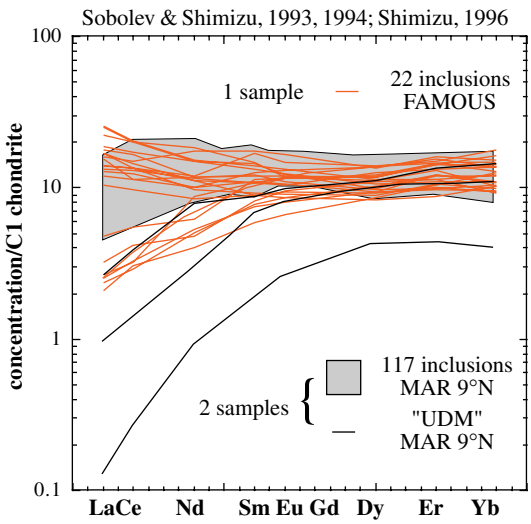

Figure 1. Chemical variation observed in melt inclusions from single hand samples; summary of results from *Shimizu* [1998] and *Sobolev and Shimizu* [1993] for samples from the Mid-Atlantic Ridge.

melt compositions varies significantly along the ridge axis. Nevertheless, the variability in trace element chemistry of the Northern EPR is comparable to that seen in melt inclusion suites from individual hand-samples.

[7] Figure 2 summarizes the composition and spatial distribution of samples from 8–15°N on the EPR. Figure 2a, compares trace element variation in off-axis lavas, including seamounts [*Niu and Batiza*, 1997], to variation in on-axis samples. All samples are basalt glasses with greater than 7 wt% MgO. The overall variation in highly incompatible elements (e.g. Ba, Th, U) is approximately two orders of magnitude in concentration while the rare earth elements (REE's) show variability similar to that seen in melt inclusions (Figure 1). Moreover, the range of composition of melts erupted on axis is similar to that seen in the seamounts, although the seamounts demonstrate a slightly wider range of variation with a larger population of more depleted compositions.

[8] Figure 2b shows a map of sample locations, with different colors corresponding to different Ba concentrations. It suggests that there are no spatial domains in which composition varies smoothly. In many cases, trace element–enriched samples are adjacent to very depleted samples. More quantitative measures of spatial coherence, such as two point correlation functions, also show that the

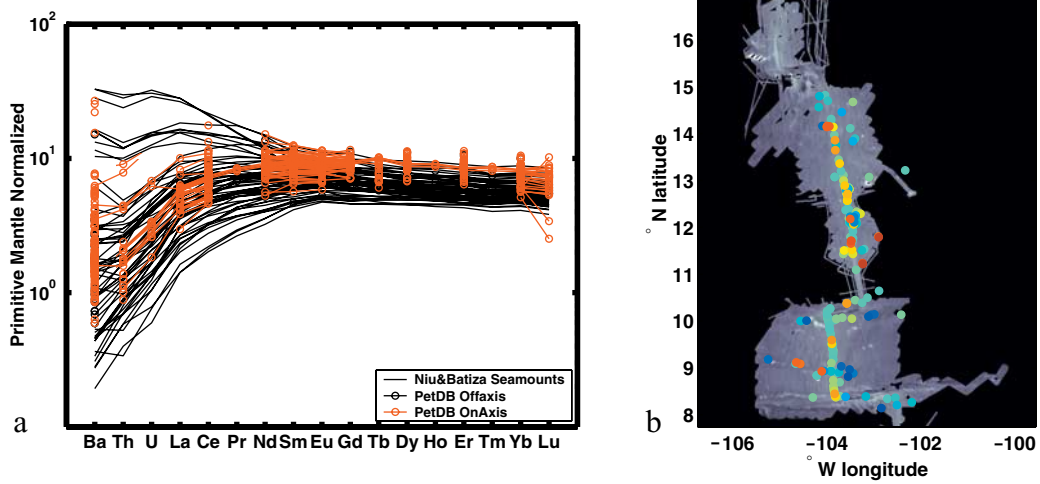

Figure 2. Chemical and spatial variation of MORB glasses with MgO > 7% from 8–15°N EPR. (a) Variability of trace element concentrations for off-axis melts (black) and on-axis melts (red). The data sources are as reported by PetDB *Lehnert et al.* [2000] with most of the off-axis analyses from *Niu and Batiza* [1997]. (b) A map showing $\log_{10}$ Ba concentration as a function of sample position. Red points are high Ba and blue points are low Ba. Note that the seamounts tend to be somewhat more depleted than the axial melts but in general the correlation between composition and location is poor.

correlation between composition and distance is low with no systematic change as a function of length scale. As might be expected from melt inclusion data, there is as much variability in samples from some individual dredge hauls (less than about 1 km on the seafloor) as there is in the entire data set.

[9] Taken together, Figures 1 and 2 suggest that partially molten regions in the mantle beneath oceanic spreading ridges can preserve significant chemical variability at all scales. While some of this variability reflects source heterogeneity, it is uncertain how much of this variability arises as a result of melting and melt transport. To answer this definitively requires systematic measurement of long-lived radiogenic isotopes on samples with known major and trace element compositions to investigate the correlations between trace element contents of lavas and isotopic variability. Given the observed lack of spatial correlation, comparing isotopes and trace elements from different samples in the same area is problematic. Surprisingly, there are relatively few areas along the global mid-ocean ridge system where isotope and trace element analyses have been made on the same samples. Where full data sets are available, the degree of correlation between trace element enrichment and isotopic enrichment is variable (see discussion). In any case, regardless of the source of variability, the preservation of heterogeneity on small scales suggests that melt transport processes in the mantle do not readily homogenize melt compositions.

1.1.3. Other Evidence for Channelized Flow

[10] Perhaps the most direct evidence for channelized flow comes from studies of ophiolites and abyssal peridotites which show evidence for "replacive dunites" embedded in residual mantle harzburgites [e.g., *Boudier and Nicolas*, 1972, 1977; *Dick*, 1977; *Boudier*, 1978; *Quick*, 1981; *Kelemen et al.*, 1992, 1995a, 2000; *Kelemen and Dick*, 1995; *Suhr*, 1999]. Geochemical arguments and field relations demonstrate that mantle dunites were channels for chemically isolated transport of melt, partly or entirely via porous flow. Several models for flow localization have been developed, ranging from mechanical instabilities driven by shear in variable viscosity solids [*Stevenson*, 1989; *Richardson*, 1998; *Hall and Parmentier*, 1998; *Connolly and Podladchikov*, 1998; *Phipps Morgan and Holtzmann*, 2001; *Spiegelman*, 2003] to physico-chemical instabilities in which high-porosity dissolution channels form via reactive melt transport in compactible media [*Kelemen et al.*, 1995b; *Aharonov et al.*, 1995; *Spiegelman et al.*, 2001]. To date, these models have focused on the mechanics of flow localization and channel formation. Here we explore the observable chemical consequences of these processes. We first review the chemical variability expected from commonly used geochemical models that do not include melt transport, then compare this behavior to that of the reactive flow models.

1.2. Variability Expected of Standard Melting Models

[11] A simple melting model for a mid-ocean ridge, is the steady state, 1-D near-fractional melting column model [e.g., *Langmuir et al.*, 1977; *Johnson and Dick*, 1992; *Sobolev and Shimizu*, 1992; *Slater et al.*, 2001] illustrated in Figure 3. These "dynamic" melting models assume that batch melting occurs up to a threshold porosity ϕ_0. Any melt produced above this threshold is then extracted instantaneously and assumed to have no further interactions with the solid. The "instantaneous" melts produced at each depth are assumed to be in chemical equilibrium with their host. In the limit $\phi_0 \rightarrow 0$, this model is identical to fractional melting.

[12] These models do not include physical mechanisms of melt transport. Nevertheless, they commonly include the assumption that instantaneous melts are mixed efficiently so that at any depth there are only two melt compositions: the instantaneous melt produced at that depth and the complete mixture of all instantaneous melts produced up to that depth. If melts are sampled only from the top of the column, the bulk of the melts will therefore be the column aggregate which shows no variability. Moreover, the aggregated melt composition for a range of values of retained porosity is nearly indistinguishable from an accumulated frac-

tional melt with the maximum degree of melting of the column.

[13] To produce significant variability from these models requires that instantaneous melts be extracted from all depths without mixing or interacting with other instantaneous melts. Figures 3b and 3c show the column aggregate and distribution of instantaneous melts from two models with different values of retained melt fraction ϕ_0. For simplicity, both calculations assume constant bulk partition coefficient and a uniform source.

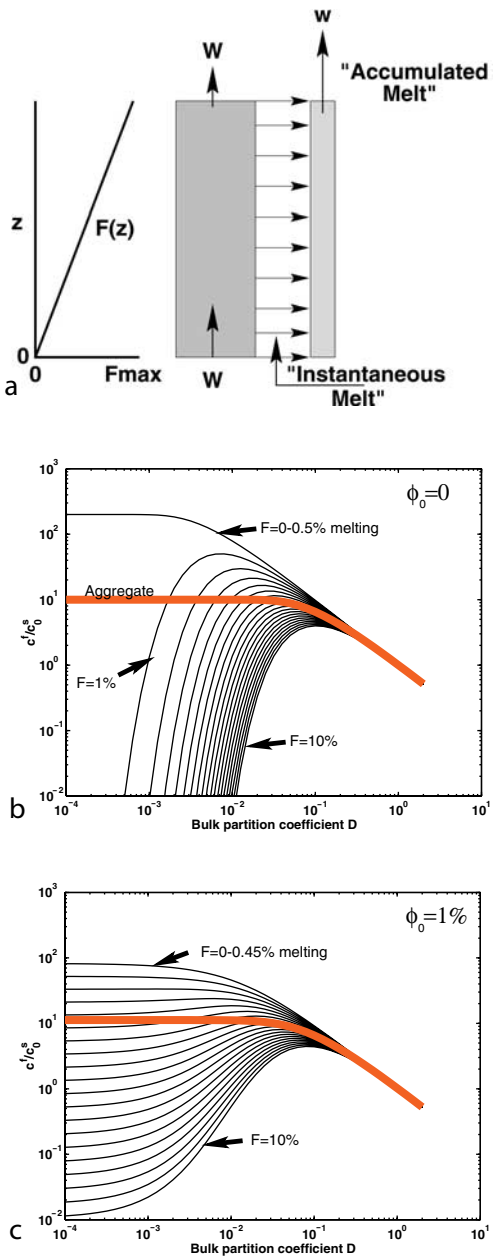

[14] Figure 3b shows the solutions for pure fractional melting $\phi_0 = 0$ while Figure 3c has a retained melt fraction $\phi_0 = 1\%$. The aggregate melts from both calculations are nearly identical and show constant concentrations relative to source of $\approx 1/F_{max}$ for all elements with partition coefficients $D \lesssim F_{max}$. In contrast, the instantaneous melts from each calculation show quite different distributions. For pure fractional melting, the instantaneous melt compositions show a strong peak in concentration for elements with $D \sim F$. Elements with crystal/liquid distribution coefficients that are smaller than the degree of melting F become extremely depleted, while elements with D's much greater than F are enriched relative to source by a factor of about $1/D$. These fractional instantaneous melt patterns are distinctly different from the compositions of melt inclusions and lavas which are nearly parallel to the mean concentrations (Figures 1 and 2). As discussed by *Slater et al.* [2001], this shows that melt inclusions are not trapped fractional melts.

[15] Instantaneous melts produced by dynamic melting with 1% retained melt (Figure 3c) are more similar to observed melt compositions. However, with 1% retained melt, the most enriched

Figure 3. (opposite) One-dimensional near-fractional melting column model. (a) Cartoon of a melting column upwelling at solid velocity W_0 with linearly increasing degree of melting $F(z)$. At each level the instantaneous melt composition for trace elements relative to source are $c^f(z)/c_0^s = \frac{1}{D^*}[(1 - F)/(1 - \phi_0)]^{(1/D^*-1)}$ where $D^* = (1 - \phi_0)D + \phi_0$ is the effective bulk partition coefficient with ϕ_0 melt retained. If these instantaneous melts are mixed completely, the aggregate melt for the entire column is $\bar{c}^f/c_0^s = (1 - \phi_0)[1 - (1 - F_{max})/(1 - \phi_0)]^{1/D^*}/(F_{max} - \phi_0)$, where F_{max} is the maximum degree of melting at the top of the column. (b) Trace element patterns for a 1-D column model with $F_{max} = 10\%$ and $\phi_0 = 0$ (pure fractional melting). Black lines are instantaneous melts shown for melting increments $dF = 0.5\%$, the red line is the mean composition after complete mixing. (c) "Dynamic" melting with $F_{max} = 10\%$ and $\phi_0 = 1\%$. Instantaneous melts shown for $dF = 0.45\%$. As discussed by *Spiegelman and Elliott* [1993], ϕ_0 is not necessarily the physical porosity, rather it is the fraction of melt that is allowed to equilibrate with the solid residue.

instantaneous melts are more enriched than observed, while calculations for U-series disequilibrium [*McKenzie*, 1985; *Williams and Gill*, 1989], which are very sensitive to the value of ϕ_0, produce excesses that are smaller than are observed in mid-ocean ridge basalts. When ϕ_0 was used as a fitting parameter to model variability in melt inclusions and lavas, *Slater et al.* [2001] found that ϕ_0 = 4–6% is required for Iceland and the Mid-Atlantic Ridge [*Shimizu*, 1998]. These best-fit values of ϕ_0 produce negligible U-series excesses in dynamic melting models, and *Slater et al.* [2001] show that they still don't fit the trace element data well.

[16] More complex two-dimensional models that approximate the melting region as an integrated set of 1-D columns of different heights (i.e. a "triangular" melting region) [e.g., *Plank and Langmuir*, 1992; *Langmuir et al.*, 1992; *McKenzie and O'Nions*, 1991; *Kinzler and Grove*, 1992a, 1992b; *Shen and Forsyth*, 1995] produce variability similar to the 1-D column models but also predict a systematic spatial distribution of melt compositions, where more enriched, smaller degree melts are found preferentially off axis. Aggregate melts produced in all of these models are similar to mean melt compositions at mid-ocean ridges. Moreover, dynamic melting models can also reproduce the observed range in composition, if large values of ϕ_0 are assumed. However, like the 1D models, the 2D models do not account for large compositional variations in a small area (e.g., melt inclusions). Nor do they explain relatively large U-series excesses in MORB, or the lack of correlation between location and lava composition on the ridge segment scale.

[17] To summarize, the overall variability of mid-ocean ridge melt compositions is better modeled by dynamic melting as compared to fractional melting. However, to interpret melt inclusions as instantaneous, dynamic melts that are trapped in olivine near the Moho, requires a physical system that extracts melts from each specific depth without allowing them to mix with melts from any other depth during transport through the mantle. To date, it has been difficult to imagine a physical mechanism for this process, although it does imply some form of channel network. In this paper, we show that, when the physics of melt extraction is included, channelization itself can provide the mechanism.

2. Geochemical Consequences of Reactive Melt Channeling

[18] This section presents results of a simple model for reactive flow and chemical transport that demonstrates how channelized flow can produce orders of magnitude variation in the concentrations of highly incompatible elements, even for idealized systems with a homogeneous source, constant bulk partition coefficients and "equilibrium transport" where trace elements maintain chemical equilibrium between the melt and solid at all times. (Disequilibrium transport is essentially fractional melting [see *Spiegelman and Elliott*, 1993].) This example is meant to be illustrative, rather than "realistic". The discussion considers additional geologically relevant processes and future work.

[19] The model is described by *Spiegelman et al.* [2001]. It consists of a two-dimensional domain, in which the solid is upwelling vertically and melting by adiabatic decompression. In addition, melt can dissolve solid material during ascent, increasing the porosity. Without reactive dissolution, this is the classic 1-D, steady state melting column, for which there are analytic solutions for porosity and chemical composition with depth [e.g., *Ribe*, 1985; *Spiegelman and Elliott*, 1993; *Spiegelman*, 2000]. In particular, for equilibrium transport, the trace element composition of the melt at any depth z is identical to that of a batch melt with degree of melting $F(z)$. This result is independent of the value of the retained porosity. Likewise, disequilibrium transport produces compositions identical to an accumulated fractional melt.

[20] Figures 4a and 4c show the numerical solutions for porosity and chemical composition for equilibrium transport. The porosity evolves to a 1-D steady state, which depends on the permeability. The permeability in this particular solution is

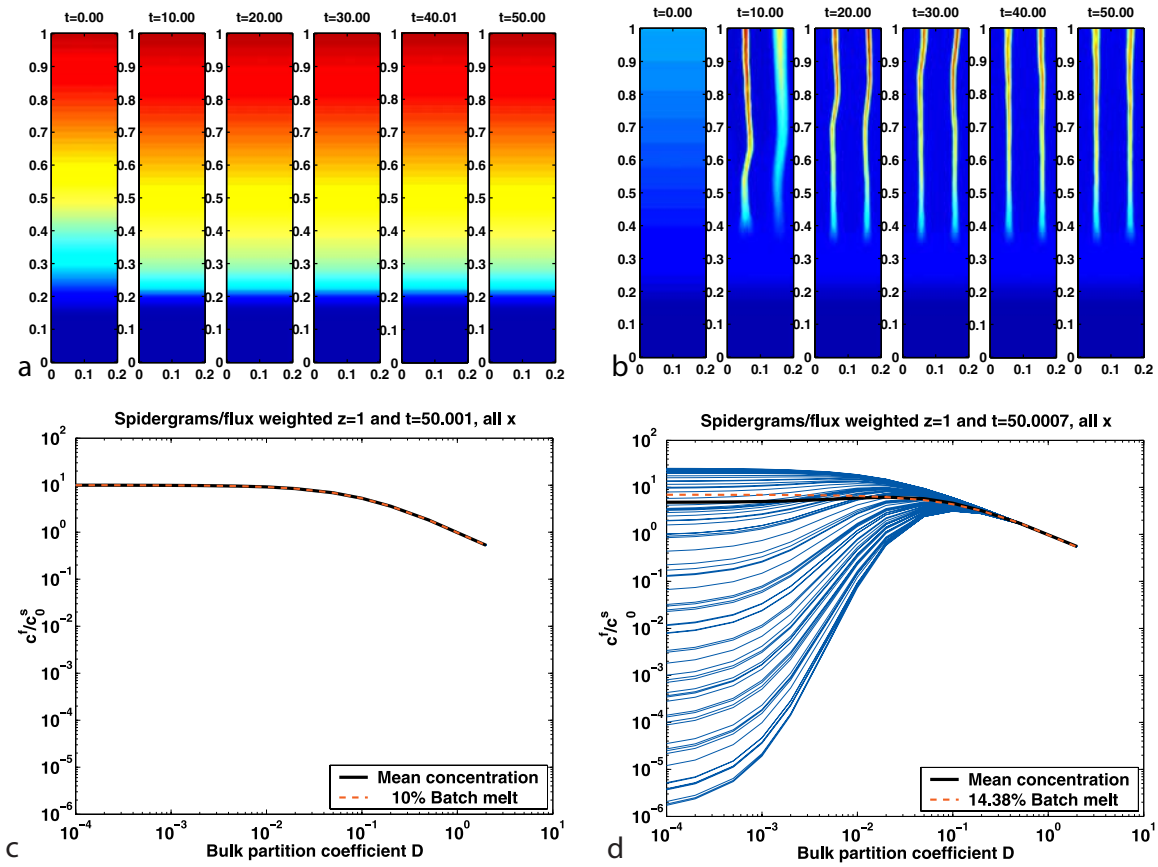

Figure 4. Evolution of porosity and chemical signatures of two upwelling models, with and without reactive dissolution. Distances are scaled to the height of the melting column and dimensionless time is scaled to the time it takes melt to cross the column at the melt reference velocity w_0 (a) Solid decompression melting but no reaction ($Da = 0$ [see *Spiegelman et al.*, 2001]). The porosity rapidly evolves to a steady state with uniform porosity at any height z and maximum porosity $\phi_{max} = 0.002$. The maximum degree of melting is 10% and the maximum ratio of melt velocity to solid velocity is $w_0/W_0 = 50$ (b) The same problem but with reactive flow ($Da = 320$, $Pe = 160$). For this problem quasi-steady state channels form rapidly with maximum porosity ~0.008. The porosity between the channels, however, has compacted to a very small value ~0.0002 making the interchannel region nearly impermeable to deeper melts. (c) Chemical signature of trace elements sampled at the top of the column with no reaction (Figure 4a) at time $t = 50$. The black lines show concentration of each tracer relative to source for each melt that exits the box (they are all the same in this problem). The red dashed line is the analytic solution for a 10% batch melt. (d) Chemical signature of channelized flow. The blue curves show the distribution of melt concentrations produced by the run in Figure 4b at $t = 50$. These curves have been sampled out of the probability distribution determined by the melt flux (i.e. compositions with large fluxes are sampled more often than those with small fluxes). The black curve is the mean of all compositions at the top of the box and the red dashed curve is the analytic solution calculated for the mean degree of melting at the top of the box (here around 14%). (Because of reactive dissolution, the maximum degree of melting for this problem is greater than the 10% in Figure 4a). Note that while the mean concentration is similar to that in Figure 4a, the range of compositional variation is extreme.

specified using the constraint that the maximum melt velocity at the top of the column is 50 times faster than the solid upwelling velocity. Conservation of mass in steady state then requires that the maximum porosity at the top of the column is $\phi_0 = F_{max}/50 = 0.2\%$ [see *Spiegelman and Elliott*, 1993]. The same solution would be found by specifying a permeability that varies as $k_\phi = k_0\phi^2$ with a prefactor

$$k_0 = \frac{50 W_0 \mu}{\phi_0 \Delta\rho g}.$$

For $\phi_0 = 0.002$, upwelling velocity ~3 cm yr^{-1} and melt buoyancy $\Delta\rho g/\mu = 5000$ (ms)$^{-1}$, the maximum

permeability is $\sim 2 \times 10^{-14}$ m^2. This compares very well with estimates of mantle permeabilities by *Von Bargen and Waff* [1986]. For example, using their formulas for permeability with $\phi = 0.002$, grain diameter $d = 3$ mm and a dihedral angle $\theta \sim 35°$ ($\Delta q \sim 0.35$) yields $k_\phi \sim 3 \times 10^{-14}$ m^2.

[21] The composition of the "erupted melts" at the top of the column in Figure 4a matches the analytic, batch melting solution to within 1 part in 10^{-3}. Unlike the dynamic melting column in Figure 3, equilibrium transport, without channels, produces a single melt composition at any depth with the most depleted melt being the melt at the top of the column (here a batch melt of 10%). Thus, without channels, the solution is rather dull and produces no variability at the top of the melting column. When reactive dissolution is added, however, all hell breaks loose. (Figures 4b and 4d).

[22] To model the effects of reactive dissolution, we follow *Spiegelman et al.* [2001] and assume that the solid is composed of two phases, which can be considered to be equivalent to pyroxene and olivine. Mantle melts produced at depth become undersaturated in pyroxene as they decompress adiabatically. Where undersaturated melts react with mantle peridotite, they dissolve pyroxene, producing a larger mass of melt, and precipitate a small amount of olivine [e.g., *Kelemen*, 1990; *Kelemen et al.*, 1990, 1995b; *Daines and Kohlstedt*, 1994]. As a first approximation, the equilibrium solubility of pyroxene is a smoothed ramp that varies from $\sim c^f_{min} = 1$ to $c^f_{max} = 1.2$ over $z_0 \leq z \leq 1$. Equilibrium solubilities greater than 1 imply incongruent reactions, in which pyroxene dissolution produces both melt and olivine; this is a more appropriate formulation than that used by *Spiegelman et al.* [2001].

[23] Because additional melt is produced in this reaction, it causes a local increase in porosity and permeability, which in turn results in a larger flux of undersaturated melt. This feedback between melt flux and dissolution leads to localization of porous flow into high-permeability dissolution channels [*Kelemen et al.*, 1995b; *Aharonov et al.*, 1995; *Spiegelman et al.*, 2001]. Figures 4a and 4b compare a calculation without reaction to one with well-developed dissolution channels. In Figure 4b, reaction causes the flow to localize into porous channels separated by low-porosity, "interchannel" regions. The low-porosity regions form because the solid matrix is deformable and the lower pressure in the channels sucks melt from the interchannel regions, causing them to compact [see *Spiegelman et al.*, 2001].

[24] The behavior of trace elements is readily calculated given the flow and melting rate fields. For clarity, we consider idealized tracers which have a constant bulk partition coefficient D and a homogeneous source. We also assume that the tracer remains in chemical equilibrium with the solid at all times, and neglect diffusion/dispersion. These assumptions permit solution for the natural log of the concentration, rather than the concentration itself. This technique is discussed by *Spiegelman* [1996] and is significantly more accurate in numerical models when concentrations vary over many orders of magnitude.

[25] Figure 4d shows the chemical variation produced in the channelized run (Figure 4b) at $t = 50$ and demonstrates seven orders of magnitude variation in incompatible element concentration. Melts range from 3–4 times more enriched than the mean to ultra-depleted melts a few orders of magnitude more depleted than the mean. The distribution is skewed, with a much larger range of incompatible element abundance below the mean, compared to the range above the mean. The mean composition of erupted melts is similar to the output of a 1-D column model with the same F_{max}. However, the distribution of individual melt compositions sampled at the top of the model domain is dramatically different.

[26] The source of the large compositional variation in Figure 4d is clear when we consider the spatial distribution of flux and composition. Figure 5 compares profiles of vertical melt flux and melt concentration as a function of distance across the top of Figure 4b at $t = 50$. The channels have large peaks in flux, flanked by compacted regions with negligible flux. They also show strong peaks in trace element concentration. However, the compositional peaks are narrower than the flux peaks, with the width of the concentration profile dependent on

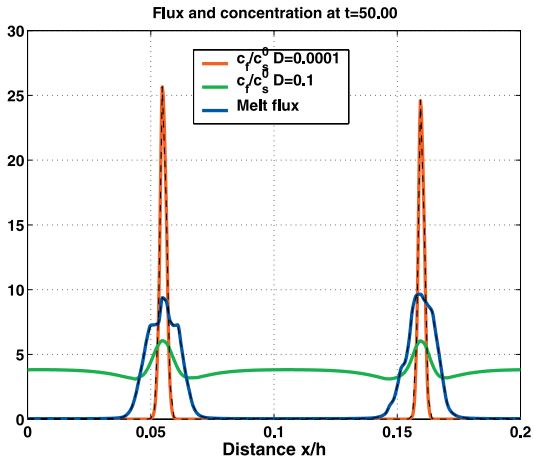

Figure 5. Comparison of variation in melt flux and variation in composition at the top of a channelized run. The blue curve shows the vertical melt flux ϕw at the top of the box shown in Figure 4b at time $t = 50$. The red curve shows the concentration of a very incompatible tracer ($D = 0.0001$) in the melt relative to source (c^f/c_0^s). The green curve shows melt concentrations normalized to source for a moderately incompatible tracer with $D = 0.1$. Note that the compositional peaks are narrower than the flux peak due to lateral advection of depleted melt from the interchannel regions into the channels. Highly incompatible elements show larger depletions between the channels and have sharper peaks. Note that the concentration at the center of the channel is more enriched than the mean concentration for the same element (here $\bar{c}^f/c_0^s \sim 7$).

partition coefficient. Highly incompatible elements (e.g. $D = 0.0001$) have narrower peaks than moderately incompatible elements ($D = 0.1$). This produces chemical distributions across the channels in which the channel centers have a large flux of enriched melts (with concentrations ~3–4 times the mean concentration) while the channel edges have a significant flux of extremely depleted melts.

[27] The presence of depleted melts within the channel edges is a natural consequence of channel formation in compactible material. Figure 4b shows that channel formation is accompanied by interchannel compaction such that interchannel regions have low porosity (here ~0.02%) and therefore low permeability. As a result, the interchannel regions almost completely exclude the ascent of deeper melts. Nevertheless, the solid is undergoing decompression melting everywhere. Melts produced between the channels have compositions similar to instantaneous fractional or dynamic melts, and become highly depleted at shallow depths. Shallow, ultra-depleted melts are drawn into the channels by the lower melt pressure in the channels. This advection of interchannel melts toward the channels produces channel edges that are extremely depleted in highly incompatible elements.

[28] The consequence of this process is that every channel contains a full spectrum of concentrations from extremely depleted to moderately enriched. In effect, the vertical distribution of instantaneous melt compositions due to polybaric decompression melting has been transposed into horizontal chemical structure across each channel. The centers of the channels preserve mixtures of enriched melts produced at depth while the edges preserve depleted instantaneous melts from shallower depths. In classical dynamic melting models, all of these melts are assumed to be homogenized into a single "aggregate melt" composition. However, when the fluid mechanics of flow in porous media is considered, much of the chemical variability produced by melting can be preserved by slow laminar flow. Moreover, because dunite channels in the mantle may only be 1–100 m in width and spaced 1–1000 meters apart [*Kelemen et al.*, 1995a, 2000; *Kelemen and Dick*, 1995; *Braun and Kelemen*, 2002], this implies that large ranges of compositional variation can be produced and preserved by melt extraction processes over small length scales.

[29] This mechanism may explain how crystals within a single pillow lava can trap variable melt inclusions. If the channels deliver melts across the Moho with highly variable concentrations on the 10 m scale, it becomes straightforward for crystals formed near the Moho to capture this variability. At shallower depths within the crust, mixing in melt lenses and dikes reduces the variability of erupted lavas.

[30] This model demonstrates that several orders of magnitude of variation in incompatible element concentration can be generated just by incorporating the physics of channelized flow in a homogeneous, near steady state, 1-D model of a melting column. Figure 6 shows some additional, time-dependent behavior. Most notably, small changes in the configuration of the channel network can

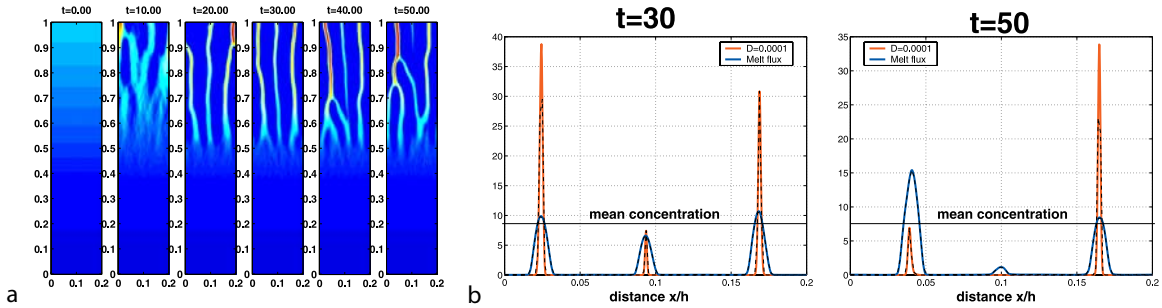

Figure 6. Time-dependent evolution of porosity and composition in channels. Animations of this and other runs can be found at http://www.ldeo.columbia.edu/~mspieg/ReactiveFlow/. (a) Evolution of porosity. While there are always approximately three channels near the top of this model, their depth extent and positions change over time. This can lead to temporal variation in flux and chemistry at any point along the top of the model. (b) Flux and composition for an element with $D = 0.0001$ at the top of the column showing the three channels at times $t = 30$ and $t = 50$ in Figure 6a. In particular, note the left most channel at $t = 30$ extends to relatively great depth and has a large flux of enriched material. At time $t = 50$ however, this channel has become connected to three other channels carrying more depleted material, producing a large flux of depleted material at the same location. Despite this local change from enriched to depleted melts, the overall variability at the top of the entire model domain is nearly constant, and comparable to Figure 4d.

result in significant changes in composition at a single point along the top of the model over timescales smaller than the melt extraction time (e.g., 24,000 years for melt traveling 50 times faster than the solid, solid upwelling over a distance of 60 km, and a solid upwelling rate of 0.05 m/year). Temporal changes in this calculation, however, could be on timescales longer than single eruption events lasting a few years to tens of years [*Reiners*, 2002]. As a result of this time dependence, individual channels can change their mean compositions from enriched to depleted when and where they become separated from deep sources. Thus time dependence introduces another, larger scale of spatial variability, equivalent to the channel spacing, that may account for some of the variability seen in erupted lavas on intermediate length scales. Temporal variation of lava composition at a given eruptive site is an important qualitative feature of volcanic systems that is difficult to understand if we only consider the flow of the upwelling, solid mantle. However, the addition of a physically consistent plumbing system provides a framework for understanding these features.

3. Discussion

3.1. Controls on Variability

[31] The calculated variability in Figure 4b is considerably larger than that seen in natural systems (Figures 1 and 2). Questions remain as to what accounts for the differences and what it may tell us about the behavior of partially molten systems.

3.1.1. Sensitivity to Channel Structure

[32] One possibility is that the variability is sensitive to the depth and efficiency of channeling. Figure 7 shows three high-resolution, single-channel calculations that have all the same parameters as Figure 4b except for the "compaction porosity," ϕ_c which controls the bulk viscosity (ease of compaction) of the matrix at small porosities [e.g., see *Spiegelman et al.*, 2001, equation (12), Figure 6]. Systems that compact easily produce smaller inner channel porosities, more flow localization and deeper channel initiation. All of these effects lead to larger variability in highly incompatible elements (Figure 7a). Systems with shorter channels and larger interchannel porosities have smaller variability.

[33] Figure 7 shows that small changes in the channel structure can lead to orders of magnitude differences in chemical variability even though the mean melt composition in all of these calculations is similar. Moreover, while the distributions of incompatible elements are qualitatively similar to those produced by dynamic melting models, the physical parameters required to produce them are significantly different. For example, the maximum

porosity in all of these models is still less than 1%, and the interchannel regions have porosities as low as 0.04% (Figure 7a) to 0.08% (Figure 7c), yet the model results show variability similar to dynamic melting models that retain more than 1% melt everywhere in the melting column. Even very small interchannel porosities produce melt compositions that are sub-parallel to the aggregate melt and do not resemble pure fractional melts (Figure 3b). Furthermore, unlike the large retained melt fractions required to produce such melt compositions in dynamic melting models, these small interchannel porosities are consistent with a reactive flow origin for the U-series disequilibrium observed in MORB [*Jull et al.*, 2002].

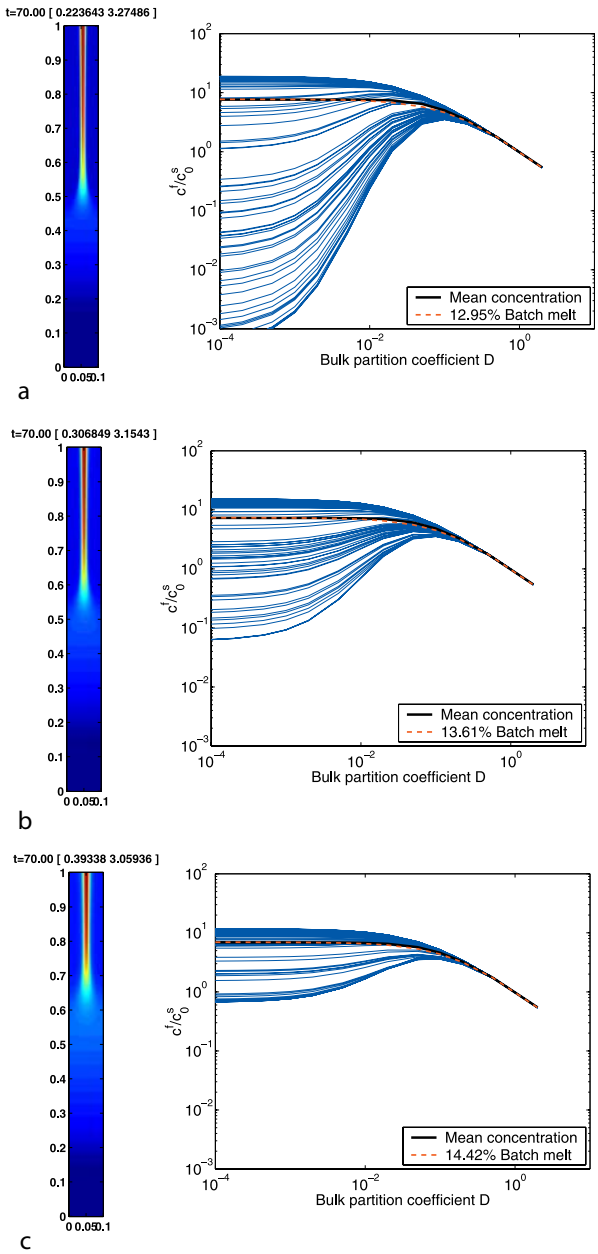

Figure 7. (opposite) Chemical variability in three high-resolution (257 × 641 grid points), single channel calculations, in which channels extend to different depths within the melting column. These calculations have the same parameters as Figure 4b except for the compaction porosity ϕ_c which controls the bulk viscosity of the matrix at low porosities [see *Spiegelman et al.*, 2001]. Results can be understood in terms of the parameter ϕ_c/ϕ_0, which is the compaction porosity relative to the reference porosity at the top of the domain in the absence of channels. Figure 4b has $\phi_c/\phi_0 = 0.1$. (a) $\phi_c/\phi_0 = .2$. The channels begin about halfway up the box and the minimum interchannel porosity is $.22\phi_0$ producing ~4 orders of magnitude variation in highly incompatible element concentration. (b) $\phi_c/\phi_0 = 0.3$, producing 2 orders of magnitude variation in highly incompatible element concentration. (c) $\phi_c/\phi_0 = 0.4$. Brackets above each porosity image give $[\phi_{min}/\phi_0\ \phi_{max}/\phi_0]$ at the top of the column.

3.1.2. Diffusion/Dispersion

[35] Another possibility for reducing model variance is molecular diffusion and/or hydrodynamic dispersion. While the models presented in this paper include diffusion in the reactive "major elements", they do not, at present, incorporate diffusion of trace elements. However, the consequences of diffusion/dispersion can be estimated.

[36] Using an argument similar to that of *Spiegelman and Kenyon* [1992], we can estimate a diffusive Damköhler number which considers the importance of diffusion across the channels relative to advective transport along the channels. The Damköhler number

$$\mathrm{Da}_D = \frac{\mathcal{D}_{\mathrm{eff}} l}{w_0 d^2} \tag{1}$$

is the time it takes for a tracer to be transported a distance l along the channel at speed w_0 divided by

the time it takes to diffuse across a channel of width d given an effective diffusivity $\mathcal{D}_{\text{eff}}$. ($1/\text{Da}_D$ is identical to what we called a Peclet number in *Spiegelman and Kenyon* [1992].) The effective diffusivity includes molecular diffusion and hydrodynamic dispersion. Systems with $Da_D \lesssim 0.1$ have negligible dispersion [*Spiegelman and Kenyon*, 1992]. Rearranging equation (1), we can estimate the width of channels that can preserve their internal chemical structure and will not be homogenized by diffusion and dispersion. This width is

$$d \geq \sqrt{\frac{10\mathcal{D}_{\text{eff}} l}{w_0}} \tag{2}$$

[37] If we assume that the melt velocity is approximately 50 times the solid upwelling velocity (i.e $w_0 \sim 1.5$ m yr^{-1} = 5 × 10^{-8} m s^{-1}), use values of molecular diffusivity for rare earth elements in Jadeite/Diopside melts of $\mathcal{D}_m \sim 10^{-11}$ m^2 s^{-1} [*Nakamura and Kushiro*, 1998] and assume that melts have traveled at least 30 km (10 kb) in channels, then equation (2) suggests that channels wider than ~10 m will be able to preserve their internal variability against diffusion. A similar result is reported by *Braun and Kelemen* [2002] (who also provide data on the size/frequency relationships of dunite channels in the mantle section of the Oman ophiolite).

[38] Of course, in porous media, hydrodynamic dispersion outweighs molecular diffusion at sufficiently large velocities. We can estimate these effects as well. *Bear* [1988] gives relationships for the ratio of the total longitudinal dispersion to molecular diffusion $\mathcal{D}_l/\mathcal{D}_m$ as a function of the grain-scale Peclet number

$$Pe_a = \frac{w_0 a}{\mathcal{D}_m} \tag{3}$$

where a is the grain radius. For $Pe_a \lesssim 1$, $\mathcal{D}_l \approx \mathcal{D}_m$ but for $Pe_a > 1$ then $\mathcal{D}_l \approx Pe_a\mathcal{D}_m$ which is actually independent of molecular diffusivity. Assuming a grain size of 1 mm and the parameters used above, $Pe_a \sim 5$. In this regime, the Damköhler number is also independent of melt velocity and we can estimate the minimum channel width as $d = \sqrt{10al}$ ≈ 17 m which is similar to the previous estimate. This may be an overestimate of the dispersion, and therefore of the required channel width as the longitudinal dispersivity tends to be larger than the transverse diffusivity which controls chemical spreading across the channels.

[39] Moreover, these estimates may also be conservative because they neglect the lateral advection of depleted melts into the channels, which counteracts diffusive spreading. Again, we can estimate this effect using another Peclet number

$$\text{Pe}_h = \frac{u_0 d}{\mathcal{D}_{\text{eff}}} \tag{4}$$

which measures the importance of horizontal advection at melt velocity u_0 to horizontal diffusion/dispersion. For $Pe_h \gtrsim 10$, advection dominates over diffusion. Using the parameters for a 10 m wide channel from the previous few paragraphs suggests that a horizontal component of velocity $u_0 \gtrsim 2$ mm yr^{-1}, is sufficient to support horizontal concentration gradients. This velocity is significantly smaller than the solid upwelling velocity, while the horizontal component of velocity near the channel edges in Figure 7b is approximately 5 times faster than the solid upwelling velocity. This suggests that lateral advection should be able to sustain channel variability despite the homogenizing effects of diffusion/dispersion.

[40] Future work will check these simple scaling arguments by explicitly including dispersion. If the scaling arguments are reasonable, however, they suggest that dispersion may homogenize channels <5–10 m wide while allowing significant variability to be preserved in larger channels. An important test of these ideas is to look for across channel variation in field exposures such as the Oman ophiolite.

3.2. Comparison to Observations

[41] While there is considerable work to do to explore the behavior and chemical consequences of the channeling mechanism presented here, we can begin to discuss how well these models account for available observations. Comparison of the models to data, however, requires considering the partitioning behavior of specific elements. For the rare earth elements, this requires at least

Table 1. Bulk Partition Coefficients Used for Figures 8 and 9

Field	Ba	Th	U	La	Ce
Garnet	0.0001	0.0027	0.0054	0.0057	0.0105
Spinel	0.0001	0.0008	0.0010	0.0039	0.0064
	Nd	Sm	Eu	Gd	Tb
Garnet	0.0285	0.0515	0.0705	0.0962	0.1340
Spinel	0.0134	0.0170	0.0206	0.0210	0.0224
	Dy	Ho	Er	Tm	Yb
Garnet	0.1811	0.2487	0.3170	0.4634	0.6140
Spinel	0.0244	0.0246	0.0253	0.0279	0.0302

two bulk partition coefficients for each element. The first corresponds to melting in the garnet lherzolite stability field and the second in the spinel lherzolite stability field (see Table 1). This introduces another input variable, the depth of the garnet-spinel transition relative to the depth of channel initiation. (In fact, there is also continuous variation of distribution coefficients throughout a realistic melting column, due to changing proportions of olivine, orthopyroxene, and clinopyroxene, as well as spinel and garnet, in the residue. However, we have not yet attempted to incorporate this effect in the modeling described in this paper.)

[42] Figure 8 shows trace element patterns calculated from the channel structure in Figure 7b with the partition coefficients in Table 1. As before, each of these distributions is calculated by sampling the melt compositions at the top of the column weighted by the melt flux. These distributions are similar to those observed in melt inclusions and lavas (Figures 1 and 2). Highly incompatible elements show about two orders of magnitude variation, while there is about a factor of two variation for moderately incompatible elements such as Yb. Moreover the most enriched melts are only about a factor of two more enriched than the mean and there is a pronounced "tail" of ultra-depleted melts.

[43] The principal difference between Figures 8a and 8b is how the channels sample the garnet-spinel transition. In Figure 8a, channels are initiated below the garnet-spinel transition, so that the centers of the channels transport mixtures of deep melts with clear garnet signatures. In Figure 8b, channels are initiated at a depth shallower than the garnet/spinel transition, so the garnet signature is subdued. In both cases, however, the edges of the

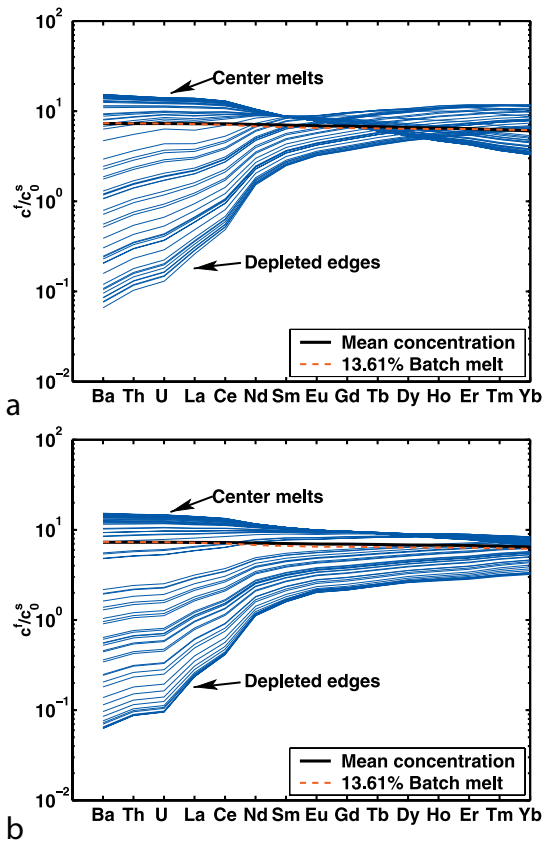

Figure 8. Melt composition distributions from initial models with a two-level partition coefficient structure to model U-Series and REE's. The background melt and solid flow field is the same as in Figure 7b with the channels beginning about halfway up the box. Compositions are calculated for highly incompatible elements (Ba, Th, U) and REE's using a two-level partition coefficient field with D_1 up to a height z_d and D_2 from z_d to the top. Specific bulk partition coefficients are given in Table 1 corresponding to garnet and spinel peridotite. Each figure shows synthetic data sets sampled out of the distribution given by the melt flux. The black line shows the mean of the distribution, the red line is the analytic solution for a batch melt with the mean degree of melting. While both models have the same mean, the distributions are different. (a) Garnet-spinel transition at $z_d = 0.6$. Channels tap into the garnet region giving enriched center melts with a clear garnet signature. (b) $z_d = 0.4$ channels occur above the gt-sp transition leaving a muted garnet signature. In both cases, the large fractionations in Yb come from including shallow, near-fractional melts from the channel edges.

channels are strongly fractionated in the heavy rare earths leading to a factor of 2 variability in Yb. The large and obvious garnet signatures in Figure 8a are not seen in mid-ocean ridge basalt. All else being equal, this suggests that channels of focused melt flow do not extend to the garnet-spinel transition. More generally, these calculations demonstrate, again, that the distribution of chemical variability, rather than the mean compositions, are a sensitive indicator of the geometry of melt transport networks.

[44] In addition to calculating the distribution of melt compositions, we can also calculate the expected distribution of "abyssal peridotite" compositions (i.e. solid residues) produced by these models. Unlike the melts, which are sampled from the distribution of compositions weighted by melt flux, the residues should be sampled from compositions weighted by area at the top of the model domain. Since most of the area is composed of interchannel regions, the majority of residues are highly depleted. Figure 9 illustrates clinopyroxene compositions that are in equilibrium with melts at the top of the column, weighted by area, and compares them to the range of clinopyroxene compositions in abyssal peridotites [e.g., *Johnson et al.*, 1990; *Johnson and Dick*, 1992] and Oman harzburgites [*Kelemen et al.*, 1997]. Again, the correspondence between model and observation is surprisingly good.

3.3. Further Tests/Further Work

[45] Figures 8 and 9 are encouraging and suggest that, possibly for the first time, there are physically consistent geochemical transport models that produce distributions of melt and solid residues similar to what is actually observed. The physical basis for these distributions is easily understood and quantifies many of the qualitative ideas inherent in "dynamic melting models". However, to produce these distributions requires including the fluid-mechanics of melt transport that control the amount of mixing between melts formed at different depths. Nevertheless, even these transport models are highly simplified with respect to possible melting regimes and it is worth reviewing, briefly, some additional tests of these models.

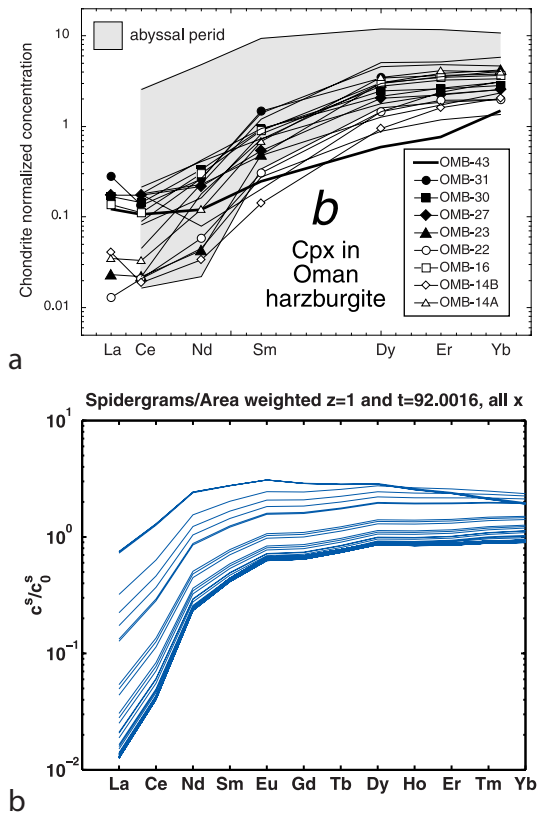

Figure 9. Comparison of observed distribution of clinopyroxene compositions in abyssal peridotites to model calculations. (a) Clinopyroxene compositions in harzburgites from the mantle section of the Oman ophiolite [*Kelemen et al.*, 1995a] superimposed on the range of compositions from abyssal peridotites [*Johnson et al.*, 1990; *Johnson and Dick*, 1992], showing the predominance of highly depleted samples. (b) Distributions of clinopyroxenes in equilibrium with melts at the top of the melting column corresponding to Figures 7b and 8b. This distribution is sampled uniformly by area (as if we were sampling residues from the top of the column) and is dominated by depleted interchannel samples.

[46] In addition to calculating distributions of stable trace elements in melts and residues, these models can also be used to calculate the effects of melt transport on uranium series (U-series) disequilibrium. Some important observations that have not been explained by traditional melting models include the correlation between Thorium excesses and elemental U/Th ratios, in which samples with high U/Th have smaller excesses [e.g., *Lundstrom et al.*, 1999]. This is particularly clear for Alvin collected samples from 9°N EPR that show correlations between (^{230}Th/^{232}Th) and

($^{238}U/^{232}Th$) as well as an intriguing anti-correlation between ($^{226}Ra/^{230}Th$) and ($^{230}Th/^{238}U$) for samples with identical Sr and Nd isotopes [*Sims et al.*, 2002]. These observations are not well explained by models of dynamic melting and ingrowth [e.g., *Williams and Gill*, 1989; *McKenzie*, 1985] which produce positive correlations in Ra versus Th. They are also not explained by open-system models of U-series excesses [*Spiegelman and Elliott*, 1993; *Lundstrom et al.*, 1995a, 1995b] that can produce Ra and Th excesses in different parts of the melting regime but, in their simplest form, do not fractionate U/Th ratios from source. Recently, *Lundstrom* [2000] and *Jull et al.* [2000, 2002] have developed simplified "two-porosity" models to allow for multiple paths for thorium and radium [see also *Iwamori*, 1993, 1994]. These models can explain the U-series observations, but require specification of many parameters. Our models should produce similar geochemical results, but with fewer input parameters combined with richer interaction between channel and inter-channel regions. Initial results [*Spiegelman and Kelemen*, 2002] of U-series calculations seem promising.

[47] In addition to explaining U-series observations, another obvious test of these models is to look for spatial variability of composition in dunites of different sizes in the mantle section of ophiolites. Such work could put constraints on the importance of dispersion in mantle melt transport, as well as determine whether variability resides at the sub-channel scale, or whether different melts are transported by different types of channels in a drainage network. However, this will be difficult, as most chemical variability in melt composition and models is in highly incompatible elements whose concentration is difficult to measure in dunites. Conversely, moderately incompatible to compatible element abundances that are easy to measure in dunites (e.g., Ca, Ti, Al, Cr, Fe, Mg, Ni), are subject to subsolidus redistribution in mantle samples, and show little variation in melts and models. Thus, a serious test of model predictions for dunites awaits trace element data on a large number (of very rare) clinopyroxenes as a function of dunite width, or measurement of slowly diffusing, highly incompatible elements (e.g. REE) in olivine.

[48] Finally there is the issue of source heterogeneity. The models shown so far demonstrate that melt transport can cause significant variability, even in melts arising from a homogeneous source. Nevertheless, it is clear from isotope data that the mantle source of mid-ocean ridge basalts is heterogeneous. Future work will investigate how a channel network samples a heterogeneous source, and how this affects correlations between trace element and isotopic variability. At this point, one can imagine several scenarios. For example, if channels nucleate on melting heterogeneities (e.g. veins/pyroxenites) it is possible that they would preserve correlations present in the source. Alternatively, if channel networks cross heterogeneities, this could destroy correlations between trace element and isotope variability.

[49] Developing models to test these ideas is possible. However, it will also be useful to develop a better understanding of correlations between trace element variability and isotopic variability in mid-ocean ridge basalt. For the few data sets where both isotope and trace element data are available on the same samples [e.g., *Niu et al.*, 1999], there is often a weak correlation between isotopic enrichment and trace element enrichment, but this tends to be weaker than the intercorrelations between trace elements and isotopes separately.

[50] The results in this paper suggest that well characterized data sets with a statistically meaningful number of analyses of trace elements and isotopes, could provide dramatic new insight into the structure of melt transport networks beneath mid-ocean ridges.

4. Conclusions

[51] 1. Field and chemical evidence both suggest that melt transport in the mantle occurs in a channelized network.

[52] 2. Physically consistent models, in which channels arise as a result of reactive melt transport,

can produce orders of magnitude variability in trace element compositions of melts on short length scales from homogeneous sources.

[53] 3. The distributions of melt compositions are similar to those produced by models of "dynamic melting". However, the physical transport models transpose the vertical variability produced by polybaric, dynamic melting into horizontal variability across individual channels. Moreover, for models that produce similar melt compositions, estimates of "retained melt fraction" from dynamic melting models are larger than melt porosities in channelized models.

[54] 4. The centers of porous melt channels in our models transport mixtures of melts produced across the melting column, including trace element–enriched, small-degree melts from depth. The edges of the channels, however, transport highly depleted, shallow melts produced in the compacting, interchannel region.

[55] 5. Slow laminar flow with negligible dispersion can preserve this lateral structure in channels $\gtrsim$10 m wide.

[56] 6. Preliminary comparison to data from melt inclusions, lavas and abyssal peridotites shows that these models produce variability similar to that observed.

[57] 7. These models suggest that important information on the structure of partially molten regions is contained in the distributions of variability.

Acknowledgments

[58] Peter Reiners and an anonymous reviewer provided very helpful reviews. This work was supported by NSF grants OCE-9530307 to Spiegelman, OCE99-070079 and OCE01-37327 to Spiegelman and Kelemen, and OCE94-16616, OCE98-19666, and OCE01-18572 to Kelemen et al. This is LDEO contribution 6402.

References

Aharonov, E., J. Whitehead, P. B. Kelemen, and M. Spiegelman, Channeling instability of upwelling melt in the mantle, *J. Geophys. Res.*, *100*, 20,433–20,450, 1995.

Bear, J., *Dynamics of Fluids in Porous Media*, Dover, Mineola, N. Y., 1988.

Boudier, F., Structure and petrology of the Lanzo peridotite massif (Piedmont Alps), *Geol. Soc. Am. Bull.*, *89*, 1574–1591, 1978.

Boudier, F., and A. Nicolas, Fusion partielle gabbroique dans la lhertzolite de Lanzo, *Bull. Suisse Mineral. Petrol.*, *52*, 39–56, 1972.

Boudier, F., and A. Nicolas, Structural controls on partial melting in the Lanzo peridotites, in *Magma Genesis*, edited by H. B. Dick, pp. 63–78, Oreg. Dep. of Geol. and Miner. Ind., Portland, 1977.

Braun, M. G., and P. B. Kelemen, Dunite distribution in the Oman ophiolite: Implications for melt flux through porous dunite conduits, *Geochem. Geophys. Geosyst.*, *3*(11), 8603, doi:10.1029/2001GC000289, 2002.

Connolly, J. A., and Y. Y. Podladchikov, Compaction-driven fluid flow in viscoelastic rock, *Geodin. Acta*, *11*, 55–84, 1998.

Daines, M. J., and D. L. Kohlstedt, The transition from porous to channelized flow due to melt-rock reaction during melt migration, *Geophys. Res. Lett.*, *21*, 145–148, 1994.

Dick, H. J. B., Partial melting in Josephine peridotite, 1, Effect on mineral-composition and its consequence for geobarometry and geothermometry, *Am. J. Sci.*, *277*, 801–832, 1977.

Hall, C., and E. M. Parmentier, Effects of melt-dependent viscosity and mantle heterogeneities on melt migration, *Eos Trans. AGU*, *79*(45), Fall Meet. Suppl., F990, 1998.

Iwamori, H., A model for disequilibrium mantle melting incorporating melt transport by porous and channel flows, *Nature*, *366*, 734–737, 1993.

Iwamori, H., ^{238}U-^{230}Th-^{226}Ra and ^{235}U-^{231}Pa disequilibria produced by mantle melting with porous and channel flows, *Earth Planet. Sci. Lett.*, *125*, 1–16, 1994.

Johnson, K. T. M., and H. J. B. Dick, Open system melting and temporal and spatial variation of peridotite and basalt at the Atlantis II fracture zone, *J. Geophys. Res.*, *97*, 9219–9241, 1992.

Johnson, K. T. M., H. J. B. Dick, and N. Shimizu, Melting in the oceanic upper mantle: An ion microprobe study of diopsides in abyssal peridotites, *J. Geophys. Res.*, *95*, 2661–2678, 1990.

Jull, M., P. B. Kelemen, and K. Sims, Constraints on melt migration from uranium-series disequilibria: An assessment of porous melt migration, *Eos Trans. AGU*, *81*(48), Fall Meet. Suppl., abstract V22C-08, 2000.

Jull, M., P. B. Kelemen, and K. Sims, Consequences of diffuse and channelled porous melt migration on uranium series disequilibria, *Geochim. Cosmochim. Acta*, *66*(23), 4133–4148, 2002.

Kelemen, P. B., Reaction between ultramafic rock and fractionating basaltic magma, 1, Phase-relations, the origin of calc-alkaline magma series, and the formation of discordant dunite, *J. Petrol.*, *31*, 51–98, 1990.

Kelemen, P. B., and H. J. B. Dick, Focused melt flow and localized deformation in the upper mantle: Juxtaposition of replacive dunite and ductile shear zones in the Josephine peridotite, SW Oregon, *J. Geophys. Res.*, *100*, 423–438, 1995.

Kelemen, P. B., D. B. Joyce, J. D. Webster, and J. R. Holloway, Reaction between ultramafic rock and fractionating basaltic magma, 2, Experimental investigation of reaction between olivine tholeiite and harzburgite at 1150°C–1050°C and 5 kb, *J. Petrol.*, *31*, 99–134, 1990.

Kelemen, P. B., H. J. Dick, and J. E. Quick, Formation of harzburgite by pervasive melt rock reaction in the upper mantle, *Nature*, *358*, 635–641, 1992.

Kelemen, P. B., N. Shimizu, and V. J. M. Salters, Extraction of mid-ocean-ridge basalt from the upwelling mantle by focused flow of melt in dunite channels, *Nature*, *375*, 747–753, 1995a.

Kelemen, P. B., J. A. Whitehead, E. Aharonov, and K. A. Jordahl, Experiments on flow focusing in soluble porous media, with applications to melt extraction from the mantle, *J. Geophys. Res.*, *100*, 475, 1995b.

Kelemen, P. B., G. Hirth, N. Shimizu, M. Spiegelman, and H. J. B. Dick, A review of melt migration processes in the adiabatically upwelling mantle beneath oceanic spreading ridges, *Philos. Trans. R. Soc. London, Ser. A*, *355*, 283–318, 1997.

Kelemen, P. B., M. Braun, and G. Hirth, Spatial distribution of melt conduits in the mantle beneath oceanic spreading ridges: Observations from the Ingalls and Oman ophiolites, *Geochem. Geophys. Geosyst.*, *1*, Paper number 1999GC000012, 2000.

Kinzler, R. J., and T. L. Grove, Primary magmas of mid-ocean ridge basalts, 1, Experiments and methods, *J. Geophys. Res.*, *97*, 6885–6906, 1992a.

Kinzler, R. J., and T. L. Grove, Primary magmas of mid-ocean ridge basalts, 2, Applications, *J. Geophys. Res.*, *97*, 6907–6926, 1992b.

Langmuir, C. H., J. F. Bender, A. E. Bence, G. N. Hanson, and S. R. Taylor, Petrogenesis of basalts from the famous area: Mid-Atlantic Ridge, *Earth Planet. Sci. Lett.*, *36*, 133–156, 1977.

Langmuir, C. H., E. Klein, and T. Plank, Petrological systematics of mid-oceanic ridge basalts: Constraints on melt generation beneath ocean ridges, in *Mantle Flow and Melt Generation at Mid-ocean Ridges*, *Geophys. Monogr. Ser.*, vol. 71, edited by J. Phipps Morgan, D. K. Blackman, and J. M. Sinton, pp. 183–280, AGU, Washington, D. C., 1992.

Lehnert, K., Y. Su, C. H. Langmuir, B. Sarbas, and U. Nohl, A global geochemical database structure for rocks, *Geochem. Geophys. Geosyst.*, *1*, Paper number 1999GC000026, 2000.

Lundstrom, C. C., Models of U-series disequilibria generation in MORB: The effects of two scales of melt porosity, *Phys. Earth Planet. Inter.*, *121*, 189–204, 2000.

Lundstrom, C. C., J. B. Gill, and B. B. Hanan, Evidence for dynamic upwelling at 33 degrees s mar from uranium series disequilibrium, *Eos Trans. AGU*, *76*, 572–573, 1995a.

Lundstrom, C. C., J. B. Gill, Q. Williams, and M. R. Perfit, Mantle melting and basalt extraction by equilibrium porous flow, *Science*, *270*, 1958–1961, 1995b.

Lundstrom, C. C., D. E. Sampson, M. R. Perfit, J. Gill, and Q. Williams, Insights into mid-ocean ridge basalt petrogenesis: U-series disequilibria from the Siqueiros Transform, Lamont Seamounts, and East Pacific Rise, *J. Geophys. Res.*, *104*, 13,035–13,048, 1999.

McKenzie, D., ^{230}Th-^{238}U disequilibrium and the melting process beneath ridge axes, *Earth Planet. Sci. Lett.*, *72*, 149–157, 1985.

McKenzie, D., and R. K. O'Nions, Partial melt distributions from inversion of rare earth element concentrations, *J. Petrol.*, *32*, 1021–1091, 1991.

Nakamura, E., and I. Kushiro, Trace element diffusion in jadeite and diopside melts at high pressures and its geochemical implication, *Geochim. Cosmochim. Acta*, *62*, 3151–3160, 1998.

Nielsen, R. L., J. Crum, R. Bourgeois, K. Hascall, L. M. Forsythe, M. R. Fisk, and D. M. Christie, Melt inclusions in high-an plagioclase from the Gorda Ridge—An example of the local diversity of Morb parent magmas, *Contrib. Mineral. Petrol.*, *122*, 34–50, 1995.

Niu, Y., and R. Batiza, Trace element evidence from seamounts for recycled oceanic crust in the eastern pacific mantle, *Earth Planet. Sci. Lett.*, *148*, 471–483, 1997.

Niu, Y., K. Collerson, R. Batiza, J. Wendt, and M. Regelous, Origin of enriched-type mid-ocean ridge basalt at ridges far from mantle plumes: The east pacific rise at 11 degrees 20′n, *J. Geophys. Res.*, *104*, 7067–7087, 1999.

Perfit, M. R., and W. W. Chadwick, Jr., Magmatism at mid-ocean ridges: Constraints from volcanological and geochemical investigations, in *Faulting and Magmatism at Mid-Ocean Ridges*, *Geophys. Monogr. Ser.*, vol. 106, edited by R. W. Buck et al., pp. 59–115, AGU, Washington, D. C., 1998.

Perfit, M. R., D. J. Fornari, M. C. Smith, J. F. Bender, C. H. Langmuir, and R. M. Haymon, Small-scale spatial and temporal variations in midocean ridge crest magmatic processes, *Geology*, *22*, 375–397, 1994a.

Perfit, M. R., M. C. Smith, D. J. Fornari, M. H. Edwards, W. I. Ridley, S. J. Goldstein, J. F. Bender, and R. M. Haymon, Detailed petrological and geochemical studies of on- and off-axis lavas from the East Pacific Rise: 9°30′–10°N, *Eos Trans. AGU*, *75*(44), Fall Meet. Suppl., F601, 1994b.

Phipps Morgan, J., and B. Holtzmann, Interactions of deformation and fluid migration, II, Melt transport in the elastic regime (Vug-waves), *Eos Trans. AGU*, *82*(47), Fall Meet. Suppl., abstract T11F-09, 2001.

Plank, T., and C. H. Langmuir, Effects of the melting regime on the composition of the oceanic crust, *J. Geophys. Res.*, *97*, 19,749–19,770, 1992.

Quick, J. E., The origin and significance of large, tabular dunite bodies in the Trinity Peridotite, northern California, *Contrib. Mineral. Petrol.*, *78*, 413–422, 1981.

Reiners, P. W., Temporal-compositional trends in intraplate basalt eruptions: Implications for mantle heterogeneity and melting processes, *Geochem. Geophys. Geosyst.*, *3*(2), 1011, doi:10.1029/2001GC000250, 2002.

Reynolds, J. R., Segment scale systematics of mid-ocean ridge magmatism and geochemistry, Ph.D. thesis, Columbia Univ./LDEO, New York, 1995.

Reynolds, J. R., and C. H. Langmuir, Identification and implications of off-axis lava flows around the East Pacific Rise, *Geo-*

chem. Geophys. Geosyst., Paper number 1999GC000033, 2000.

Reynolds, J. R., C. H. Langmuir, J. F. Bender, K. A. Kastens, and W. B. F. Ryan, Spatial and temporal variability in the geochemistry of basalts from the East Pacific Rise, *Nature*, *359*, 493–499, 1992.

Ribe, N. M., The generation and composition of partial melts in the Earth's mantle, *Earth Planet. Sci. Lett.*, *73*, 361–376, 1985.

Richardson, C. N., Melt flow in a variable viscosity matrix, *Geophys. Res. Lett.*, *25*, 1099–1102, 1998.

Saal, A., S. Hart, N. Shimizu, E. Hauri, and G. D. Layne, Pb isotopic variability in melt inclusions from oceanic island basalts, Polynesia, *Science*, *282*, 1481–1484, 1998.

Shen, Y., and D. W. Forsyth, The initial and final depths of melting beneath mid-ocean ridges, *J. Geophys. Res.*, *100*, 2211–2237, 1995.

Shimizu, N., The geochemistry of olivine-hosted melt inclusions in a FAMOUS basalt ALV519-4-1, *Phys. Earth Planet. Inter.*, *107*, 183–201, 1998.

Shimizu, N., and T. L. Grove, Geochemical studies of olivine-hosted melt inclusions from ridges and arcs, *Eos Trans. AGU*, *79*(45), Fall Meet. Suppl., F1002, 1998.

Sims, K. W. W., et al., Chemical and isotopic constraints on the generation and transport of magma beneath the East Pacific Rise, *Geochim. Cosmochim. Acta*, *66*(19), 3481–3504, 2002.

Slater, L., D. McKenzie, K. Grönvold, and N. Shimizu, Melt generation and movement beneath Theistareykir, NE Iceland, *J. Petrol.*, *42*, 1–34, 2001.

Sobolev, A. V., Melt inclusions in minerals as a source of principle petrological information, *Petrologiya*, *4*(3), 228–239, 1996. (*Petrology*, *4*, 209–220, 1996.)

Sobolev, A. V., and N. Shimizu, Superdepleted melts and ocean mantle permeability, *Dokl. Ross. Akad. Nauk*, *326*, 354–360, 1992.

Sobolev, A. V., and N. Shimizu, Ultra-depleted primary melt included in an olivine from the Mid-Atlantic Ridge, *Nature*, *363*, 151–154, 1993.

Sobolev, A. V., A. W. Hofmann, and I. K. Nikogosian, Recycled oceanic crust observed in 'ghost plagioclase' within the source of Mauna Loa lavas, *Nature*, *404*, 986–990, 2000.

Sours-Page, R., K. T. M. Johnson, R. L. Nielsen, and J. L. Karsten, Local and regional variation of MORB parent magmas: Evidence from melt inclusions from the Endeavour Segment of the Juan de Fuca Ridge, *Contrib. Mineral. Petrol.*, *134*, 342–363, 1999.

Spiegelman, M., Geochemical consequences of melt transport in 2-D: The sensitivity of trace elements to mantle dynamics, *Earth Planet. Sci. Lett.*, *139*, 115–132, 1996.

Spiegelman, M., UserCalc: A Web-based U-series calculater for mantle melting problems, *Geochem. Geophys. Geosyst.*, *1*, Paper number 1999GC000030, 2000.

Spiegelman, M., Linear analysis of melt band formation by simple shear, *Geochem. Geophys. Geosyst.*, *4*, doi:10.1029/2002GC000499, in press, 2003.

Spiegelman, M., and T. Elliott, Consequences of melt transport for U-series disequilibrium in young lavas, *Earth Planet. Sci. Lett.*, *118*, 1–20, 1993.

Spiegelman, M., and P. B. Kelemen, Highway to Hell: Geochemical consequences of channelized melt transport, *Geochim. Cosmochim. Acta*, *66*(15A), suppl. 1, A731, 2002.

Spiegelman, M., and P. Kenyon, The requirements for chemical disequilibrium during magma migration, *Earth Planet. Sci. Lett.*, *109*, 611–620, 1992.

Spiegelman, M., P. B. Kelemen, and E. Aharonov, Causes and consequences of flow organization during melt transport: The reaction infiltration instability in compactible media, *J. Geophys. Res.*, *106*, 2061–2077, 2001.

Stevenson, D. J., Spontaneous small-scale melt segregation in partial melts undergoing deformation, *Geophys. Res. Lett.*, *16*, 1067–1070, 1989.

Suhr, G., Melt migration under oceanic ridges: Inferences from reactive transport modelling of upper mantle hosted dunites, *J. Petrol.*, *40*, 575–599, 1999.

Von Bargen, N., and H. S. Waff, Permeabilities, interfacial areas and curvatures of partially molten systems: Results of numerical computations of equilibrium microstructures, *J. Geophys. Res.*, *91*, 9261–9276, 1986.

Williams, R. W., and J. B. Gill, Effects of partial melting on the ^{238}U decay series, *Geochim. Cosmochim. Acta*, *53*, 1607–1619, 1989.